Transworld Research Network
37/661 (2), Fort P.O., Trivandrum-695 023, Kerala, India

Recent Research Topics and Developments in Chemical Physics : From Quantum Scale to Macroscale, 2008: 179-196 ISBN: 978-81-7895-316-8
Editors: Andreas F. Terzis and Emmanuel Paspalakis

7 Segmental dynamics in polyethylene melts through atomistic molecular dynamics simulations

V. A. Harmandaris[1] and V. G. Mavrantzas[2]
[1]Max Planck Institute for Polymer Research, D-55128, Mainz, Germany
[2]Institute of Chemical Engineering and High Temperature Chemical Processes (FORTH- ICE/HT) & Department of Chemical Engineering, University of Patras, GR 26504, Patras, Greece

Abstract

We have studied issues related to segmental mobility and dynamics in linear polyethylene (PE) melts, using a method that relies on the execution of rather long (up to 0.5μs) atomistic molecular dynamics (MD) simulations and analytical expressions from well-established mesoscopic theories providing a link between simulation data and experimental observables. The simulations have been carried out with linear PE model systems ranging in molecular length from C_{78} to

Correspondence/Reprint request: Dr. V. G. Mavrantzas, Institute of Chemical Engineering and High Temperature Chemical Processes, (FORTH- ICE/HT) & Department of Chemical Engineering, University of Patras, GR 26504, Patras, Greece. E-mail: vlasis@chemeng.upatras.gr; Dr. V.A. Harmandaris, Max Planck Institute for Polymer Research, D-55128, Mainz, Germany E-mail: harmanda@mpip-mainz.mpg.de

C_{1000}, spanning the Rouse and the entangled regimes of polymer melt dynamics as well as the crossover from the one to the other. The following four measures of segmental dynamics have been calculated and analyzed as a function of chain length: the time autocorrelation function of dihedral angles, the single chain dynamic structure factor, the mean-square displacement of the innermost chain segments, and the relaxation of the normal modes. Our results are consistent with the generally accepted picture for a crossover from an untangled (or Rouse) to an entangled behavior as the chain length N increases above a certain value (the entanglement chain length N_e). In particular, by mapping out simulation data for the dynamic structure factor of the longest (C_{1000}) PE system onto the reptation model, a value has been extracted for the effective tube diameter in this system which is consistent with the value measured experimentally through neutron scattering experiments.

I. Introduction

Dynamics and relaxation in polymer systems occur over a wide range of time scales ranging from picoseconds (corresponding to bond length and bond angle vibrations or conformational transitions) to nanoseconds (corresponding to segmental relaxation far above T_g) and to seconds and beyond (corresponding to terminal relaxation in high molecular weight melts which governs their response to an applied flow field, or to dynamics at temperatures close to the glass transition temperature where the chain backbone is practically frozen). In polymers bearing side groups, dynamics is even richer involving additional types of motion such as librations and rotations of the side groups and bond angle bending vibrations of the pendant bonds. From the point of view of polymer theories, dynamics in rather short chain length polymer melts (with molecular length N smaller than a characteristic chain length N_e for the formation of entanglements) is well described by the Rouse model[1,2,3] wherein a chain is envisioned as a set of Brownian particles connected by harmonic springs and moving in the "sea" formed by the rest of the monomers. For longer polymer melts (with molecular length N higher than N_e), reptation is a theory that describes more successfully the polymer dynamics[2]. This theory postulates that the motion of an individual chain is practically restricted in a tube-like region as defined by the topological constraints imposed by the surrounding chains.

Experimentally, segmental dynamics is probed by neutron spin echo (NSE) measurements which calculate the coherent and incoherent dynamic structure factors $S(q,t)$.[4-10] NSE-based dynamic structure factor measurements on polyethylene[4] (for example) in the Fourier time range of t = 0.3–175 ns and for momentum transfers q between 0.05 and 0.145 $Å^{-1}$ have been used to test theoretical expressions for a number of models. Reptation theory was

documented as the only one that provided a consistent description of the NSE data.[4] Double-quantum nuclear magnetic resonance (DQ NMR) measurements are also very useful providing direct information about the translational motion of chains in the system. DQ NMR experiments, for example, have elucidated the nature of polymer chain dynamics in a polybutadiene melt far above the glass transition with the obtained experimental information about the rotational dynamics of spin pairs supporting many (but not all) aspects of the reptation model.[11]

Clearly, for a given polymer system (i.e., a system with a known chemistry and molecular architecture of the constituent chains), dynamics is strongly governed by the molecular weight M of the chains. In an effort to further elucidate this complex interplay between dynamics and molecular weight, the atomistic molecular dynamics (MD) method is used here in order to analyze the chain length dependence of the relaxation properties in linear PE melts.[12-26] Despite its limitations (most of which are associated with the problem of long relaxation times characterizing high molecular weight systems), MD is an ideal tool for investigating molecular motion at different length scales in a polymer melt and analyzing available experimental data. For example, it has been used in the past to calculate the monomer friction coefficient ζ in PE[14] and cis-1,4-PB,[18] to study the self-diffusion properties of n-alkane and cis-1,4-polyisoprene oligomer melts,[15,20] to interpret quasi-elastic neutron scattering measurements in atactic polypropylene,[19] and to exploit the dynamic behavior of more complex systems such as entangled polymers, non-linear polymers, and polymer blends.[16,18,25] In this work, emphasis is primarily given to the study of relaxation properties that are related with conformational re-arrangements and segmental mobility in PE. The rest of the chapter is therefore organized as follows: Section II presents details of the molecular model employed in the MD studies and reviews the strategy followed to extend the simulations to rather long chain length PE systems (such as the C_{1000} melt). Section III outlines key elements of the Rouse and reptation theory approaches to polymer dynamics, including their predictions for the (normalized) single-chain intermediate coherent dynamic structure factor. The results of our work for the chain length dependence of conformational dynamics, the dynamic structure factor, the mean-square displacement (msd) of chain segments, and the dynamics of the normal modes are presented in Section IV. The Chapter ends with Section V including the main conclusions of the present study and an outlook for further studies.

II. Molecular model

A united-atom description is used in the present work, with each methylene and methyl group along a PE chain considered as a single Lennard-

Jones interaction site. Non-bonded interactions are described by a Lennard-Jones potential of the form

$$V_{LJ}(r) = 4\varepsilon\left[\left(\frac{\sigma}{r}\right)^{12} - \left(\frac{\sigma}{r}\right)^{6}\right] \quad (1)$$

with ε=0.098 kcal/mol and σ=3.94Å. $V_{LJ}(r)$ describes all intermolecular site-site interactions as well as intramolecular interactions between sites separated by more than 3 bonds. A potential cutoff distance of 9.062Å is used. Attractive tail contributions are applied to both energy and pressure using standard analytical expressions that assume a uniform density distribution beyond the cut-off. A bond-bending potential of the form[27]

$$V_{bending}(\theta) = \frac{1}{2}k_{\theta}\left(\theta - \theta_0\right)^2 \quad (2)$$

is also used for every skeletal bond angle θ, with k_{θ}=115.2 kcal mol^{-1} rad^{-2} and θ_0=112^{o}. Associated with each dihedral angle ϕ is a torsional potential of the form[28]

$$V_{torsional}(\phi) = c_0 + c_1\cos\phi + c_2(\cos\phi)^2 + c_3(\cos\phi)^3 + c_4(\cos\phi)^4 + c_5(\cos\phi)^5 \quad (3)$$

with c_0 = 2.217, c_1 = 2.905, c_2 = -3.135, c_3 = -0.731, c_4 = 6.271, and c_5 = -7.527 all in kcal/mol.

Adjacent methyl and methylene groups are maintained at a fixed distance l=1.54 Å using the SHAKE method.[29]

The equations of motion have been integrated with a multiple time step algorithm (rRESPA) involving two time steps:[30] a shorter one (equal to 2 fs) for the integration of the faster degrees of freedom (bending and dihedral angles) and a larger one (equal to 10 fs) for the integration of the slower degrees of freedom (non-bonded LJ interactions). Three different systems have been studied: a 20-chain C_{78}, a 20-chain C_{156}, and a 8-chain C_{1000} PE melt, all characterized by uniform chain length distributions with a polydispersity index I of about 1.05. The overall simulation time ranged from 0.1 μs to 0.5 μs depending on the molecular lengths of the systems studied. All MD simulations have been conducted in the canonical (NVT) statistical ensemble, at T=450K and density equal to 0.775 g cm^{-3}, 0.790 g cm^{-3} and 0.800 g cm^{-3} for the C_{78}, C_{156} and C_{1000} PE melts, respectively. Initial configurations were obtained from EBMC simulations[31] of the same model systems at the same T and P conditions. Pre-equilibration with the EBMC algorithm was necessary in order to save computational time by having the MD simulation started from an

initial configuration that had been thoroughly equilibrated at all length scales. The execution of the MD algorithm then allows one to accumulate a large number of dynamical trajectories for the subsequent calculation of the dynamic properties and the mapping onto the mesoscopic models (Rouse and reptation). Through this multi-stage simulation approach,[14] one can overcome part of the problem of long relaxation times plaguing brute-force dynamic simulations of high polymer melts thus "pushing up" atomistic MD simulations of PE systems to longer melts such as the C_{1000} system studied here (with a molecular length N equal to almost ten times the entanglement molecular length N_e of PE).

III. Polymer dynamics – Some theoretical approaches

A. Unentangled polymer melts: The Rouse model

Assume a polymer chain consisting of N monomers (or Kuhn segments) with coordinates $\mathbf{R}_i$, i = 1, 2, …, N. The Rouse model is formulated in terms of the normal coordinates or modes $\mathbf{X}_p$ with p = 0, 1, 2, …, N-1, each of which is capable of independent motion,[2] defined by:

$$\mathbf{X}_p = \sum_{n=1}^{N} \Omega_{np} \mathbf{R}_{n-1}, \qquad \Omega_{np} = \sqrt{\frac{2-\delta_{p0}}{N}} \cos\left(\frac{(n-1/2)\, p\pi}{N} \right) \tag{4}$$

The (independent) motion of each normal mode is described by a Langevin equation in which excluded volume effects and hydrodynamic interactions are disregarded. Thus, the Rouse model leads to the following expressions for the time autocorrelation functions of the normal modes with p>0:

$$\left\langle \mathbf{X}_p(t) \cdot \mathbf{X}_p(0) \right\rangle = \exp\left(-\frac{t}{\tau_p} \right) \tag{5}$$

where

$$\tau_p = \frac{\tau_1}{p^2}\ , \qquad \tau_1 \equiv \tau_R = \frac{\zeta N^2 b^2}{3\pi^2 k_B T} \tag{6}$$

define the spectrum of relaxation times. In the above equations, τ_R is the longest (or the Rouse) relaxation time, ζ the monomer friction coefficient and b the effective bond length (i.e., the length of the Kuhn segment) along the chain. Based on these definitions and the assumption of a Gaussian distribution for the end-to-end vector of the chain, the equilibrium mean-square chain end-to-end distance is given by $\langle R^2 \rangle = Nb^2$.

The Rouse model leads also to a closed form expression for the mean square displacement (msd) of chain segments, $\phi(n,t)$, defined as:

$$\phi(n,t) \equiv \left\langle \left(\mathbf{R}(n,t) - \mathbf{R}(n,0) \right)^2 \right\rangle \cdot \tag{7}$$

Using that the coordinate $\mathbf{X}_0$ represents the position of the center of mass, the Rouse model calculates $\phi(n,t)$ as:[2]

$$\phi(n,t) = 6Dt + \frac{4\left\langle R^2 \right\rangle}{\pi^2} \sum_{p=1}^{\infty} \frac{1}{p^2} \cos\left(\frac{p\pi n}{N} \right)^2 \left[1 - \exp\left(-tp^2 / \tau_R \right) \right] \cdot \tag{8}$$

For very short times ($t < \tau_R$), the sum over p on the right-hand-side of eq. (8) is dominated by the terms with large p and $\phi(n,t)$ comes out to scale with t as $\sim t^{1/2}$. On the other hand, for longer times ($t >> \tau_R$), the term in eq. (8) involving the summation over p may be neglected and $\phi(n,t)$ is found to scale with t as $\sim t$.

Of interest is also the expression derived by the Rouse model for the single-chain intermediate dynamic structure factor $S(q,t)$, a quantity which is experimentally accessible. $S(q,t)$ is defined as

$$S(q,t) \equiv \sum_{n,m} \left\langle \exp\left[i\mathbf{q} \cdot \mathbf{R}_{nm}(t) \right] \right\rangle \tag{9}$$

where $\mathbf{q}$ is the scattering vector and n, m denote atoms belonging to the same chain. In eq. (9), $\mathbf{R}_{nm}(t)$ is the displacement vector between chain segments n, m defined as:

$$\mathbf{R}_{nm}(t) \equiv \mathbf{R}(n,t) - \mathbf{R}(m,0) \ , \tag{10}$$

with $\mathbf{R}(n,t)$ denoting the position vector of chain segment n at time t and $\mathbf{R}(m,0)$ the position vector of chain segment m at time 0. For an isotropic (melt) sample, eq. (9) reduces to[2]

$$S(q,t) = \sum_{n,m} \left\langle \sin\left[qR_{nm}(t) \right] / qR_{nm}(t) \right\rangle \tag{11}$$

where $\mathbf{R}_{nm}(t)$ is the magnitude of $R_{nm}(t)$. In fact, what is measured directly in the neutron spin echo (NSE) experiments is the normalized single-chain intermediate coherent dynamic structure factor; this is defined as:

$$S'(q,t) = \frac{S(q,t)}{S(q,0)} = \frac{\sum_{n,m} \left\langle \sin\left[qR_{nm}(t)\right] / qR_{nm}(t) \right\rangle}{\sum_{n,m} \left\langle \sin\left[qR_{nm}(0)\right] / qR_{nm}(0) \right\rangle} \tag{12}$$

By further assuming that segmental displacements follow a Gaussian distribution, the single-chain dynamic structure factor simplifies to

$$S(q,t) \equiv \sum_{n,m} \exp\left[-\frac{q^2}{6} \phi(n,m;t) \right] \tag{13}$$

where $\phi(n,m;t)$ is the time correlation function of chain segments *n* and *m*:

$$\phi(n,m;t) \equiv \left\langle \left(\mathbf{R}(n,t) - \mathbf{R}(m,0) \right)^2 \right\rangle \tag{14}$$

Further analysis requires the explicit calculation of the quantity $\phi(n,m;t)$. For the finite (i.e., the discrete) Rouse model, such a derivation gives:[16]

$$S(q,t) = \frac{1}{N} \exp\left[-q^2 Dt \right] \sum_{n,m}^{N} \exp\left\{ -\frac{q^2 b^2}{12N} \sum_{p=1}^{N-1} \frac{1}{\sin^2\left(\frac{p\pi}{2N}\right)} \left[\cos\left(\frac{p\pi(m-1/2)}{N} \right) - \cos\left(\frac{p\pi(n-1/2)}{N} \right) \right]^2 \right. \tag{15}$$

$$\left. - \frac{q^2 b^2}{6N} \sum_{p=1}^{N} \frac{1}{\sin^2\left(\frac{p\pi}{2N}\right)} \cos\left(\frac{p\pi(n-1/2)}{N} \right) \cos\left(\frac{p\pi(m-1/2)}{N} \right) \left[1 - \exp\left(-\frac{t}{\tau_p} \right) \right] \right\}$$

where *D* denotes the the self diffusion constant of the chain center-of-mass.

B. Entangled polymer melts: Reptation theory

Experimentally, the Rouse model described in the previous section is found to successfully describe the dynamic properties of polymer melts as long as their molecular length is smaller than the characteristic molecular length for the formation of entanglements, N_e. For polymer melts with chain length *N* greater than N_e, a more successful model of polymer dynamics is provided by the reptation theory. According to this theory, the motion of a chain in a high molecular weight polymer melt is restricted within a tube-like region formed by the topological (uncrossability) constraints of (or

entanglements with) the surrounding environment (other polymer chains).[2] Key in the reptation theory is the notion of the primitive path: this is defined as the shortest path connecting the two ends of the chain and having the same topology as the chain itself relative to the topological constraints or obstacles. The conformation of the primitive path is Gaussian on a large length-scale and its step length is denoted as α. The contour length L of the primitive path is then given as $L=<R^2>/a$ or $L=Nb^2/a$. In the reptation model, the step length a is taken to be commensurate with the diameter of the effective tube, i.e., it provides a measure of the mesh size of the underlying entanglement network (the average distance between topological constraints). For this reason, α is quite often referred to also as the *effective* tube diameter.

In general, mapping atomistic MD data onto the reptation model has been an outstanding issue in polymer research community because it involves the reduction of atomistic trajectories to primitive paths (group of conformations which are accessible to each other without violating the topological constraints). It was addressed only very recently through the development of three different methods for calculating chain paths that are either in mechanical equilibrium or of the shortest disconnected path in the Euclidean sense.[32,33,34]

Of interest here are the predictions of the reptation model for the msd of chain segments. If the segmental $\phi(n,t)$-versus-t curve is plotted on a log-log plot, reptation theory predicts 4 distinct regions of dynamics with the following scalings:

- A very short time regime, for times $t < \tau_e$ where $\tau_e = \frac{\alpha^4 \zeta}{k_B T b^2}$ denotes the time at which the segmental displacement becomes comparable to the tube diameter, for which $\phi(n,t) \sim t^{1/2}$.
- An intermediate time regime, for times $\tau_e < t < \tau_R$, where $\phi(n,t)$ scales as $\phi(n,t) \sim t^{1/4}$ as a consequence of two effects, the Rouse-like diffusion and the tube constraints.
- A second intermediate time regime, for times $\tau_R < t < \tau_d$ where $\tau_d = \frac{\zeta N^3 b^4}{\pi^2 k_B T \alpha^2}$ denotes the time that corresponds to the disentanglement of the chain from the tube, for which the behavior of the chain agrees with that predicted by the primitive chain dynamics equations and $\phi(n,t) \sim t^{1/2}$.
- A long time region, for time $t > \tau_d$, for which the dynamics is governed by the reptation process and $\phi(n,t) \sim t^1$.

In the deep-reptation regime, one can also work out an analytical expression for the single-chain dynamic structure factor, the final result being:[4,35]

$$\frac{S(q,t)}{S(q,0)} = \left\{1-\exp\left[-(q\alpha/6)^2\right]\right\}\exp(t/\tau_0)\mathrm{erfc}\left(\sqrt{t/\tau_0}\right) + \frac{8}{\pi^2}\exp\left[-(q\alpha/6)^2\right]\sum_{p=odd}^{\infty}\frac{1}{p^2}\exp\left(-\frac{p^2 t}{\tau_d}\right) \quad (16)$$

with τ_0 a short time constant given as $\tau_0 = 12\zeta / k_B T b^2 q^4$. Eq. (16) for the single-chain dynamic structure factor has been derived on the basis of negligible contour length fluctuation and constraint release phenomena, so it should be expected to be applicable only in high molecular weight melts (chain length N>100 N_e) where these phenomena are less important, and for wave-vectors q such that: $1/\sqrt{\langle R^2 \rangle} << q/2\pi << 1/\alpha$.

IV. Results

A. Conformational dynamics

Conformational relaxation in a polymer system can be quantified in terms of the torsional autocorrelation function defined as:

$$P(\phi(t)) = \frac{\langle \cos(\phi(t))\rangle\langle \cos(\phi(t))\rangle - \langle(\cos(\phi(t)))\rangle^2}{\langle \cos(\phi(0))\rangle\langle \cos(\phi(0))\rangle - \langle(\cos(\phi(t)))\rangle^2} \quad (17)$$

where $\phi(t)$ is the dihedral angle. The decay of $P(\phi(t))$ for the dihedral angles along the chain backbones of the three systems studied here (C_{78}, C_{156}, and C_{1000}) is shown in Figure 1 by the symbols. Although the shorter molecular weight system, C_{78}, is characterized by a faster local dynamics, for the other two systems, C_{156}, and C_{1000}, the decay of $P(\phi(t))$ to zero is practically identical (within the error bars) suggesting that above a certain chain length, the rate with which the function $P(\phi(t))$ decorrelates in a linear PE melt is independent of the chain length N. Also shown in Figure 1 by the continuous lines are the best fits to the $P(\phi(t))$-vs.-t data with stretched exponential functions of the form $P(\phi(t)) = \exp\left(-(t/t_c)^{\beta}\right)$ which are observed to follow the simulation curves remarkably accurately. The characteristic relaxation times t_c and stretching exponents β obtained by the fittings are t_c = 3.9 ps and β = 0.77 for the C_{78} system, and t_c = 5.9 ps and β = 0.80 for the C_{156} and C_{1000} systems. The corresponding correlation times τ (integrals under the $P(\phi(t))$-vs.-t curves) are τ = 5.16 ps for the C_{78} system, and to τ = 6.95 ps for the C_{156} and C_{1000} systems.

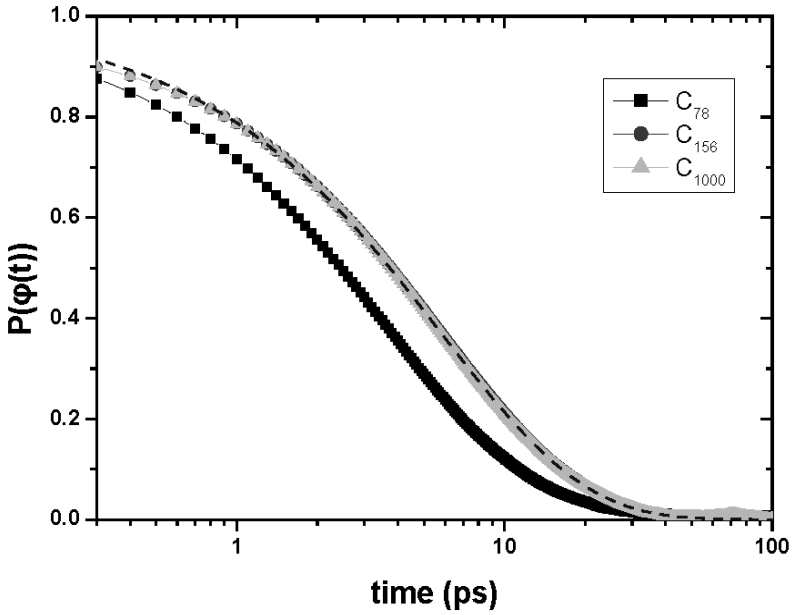

Figure 1. Torsional time autocorrelation functions in the three PE systems (symbols) and their stretched exponential fits (lines).

B. Dynamic structure factor

Parts a and b of Figure 2 present results for the normalized single-chain intermediate dynamic structure factor, $S'(q,t)$, for various values of the scattering vector q (= 0.04 Å^{-1}, 0.16 Å^{-1} and 0.28 Å^{-1}) as obtained directly from the MD simulations using eq. (12) (symbols) for the two shorter systems, C_{78} and C_{156}, studied in this work. Also presented in these figures are the predictions of eq. (15) using either the finite Rouse model (solid lines) or an improvement of the Rouse model (the semiflexible chain model) that incorporates chain stiffness (dashed lines) for the two systems.[3] The number of statistically independent segments N and the effective length b of the statistical segment entering these expressions were calculated from the MD simulation data using the following expressions for the chain mean-square end-to-end distance and maximum contour length, respectively: $\langle R^2 \rangle = Nb^2$ and $R_{max} = Nb$.

It is clear from Figure 2, that the C_{78} PE melt follows quite faithfully the Rouse dynamics for small q values (e.g., for q=0.04 Å^{-1}) corresponding to the length scale of the chain end-to-end distance. This is in agreement with earlier investigations of the zero-shear rate viscosity, diffusion coefficient, normal-mode analysis and friction coefficient.[14] The plots of the single-chain dynamic structure factor presented in Figure 2 provide a further confirmation of this behavior, for wave vectors whose length q is below about 0.16 Å^{-1}. For higher q values, the atomistic MD data show that $S'(q,t)$ decays slower than what is predicted by the Rouse model, for all times. In fact, the deviations get larger and larger with increasing q, which suggests that the dynamics of shorter

(a)

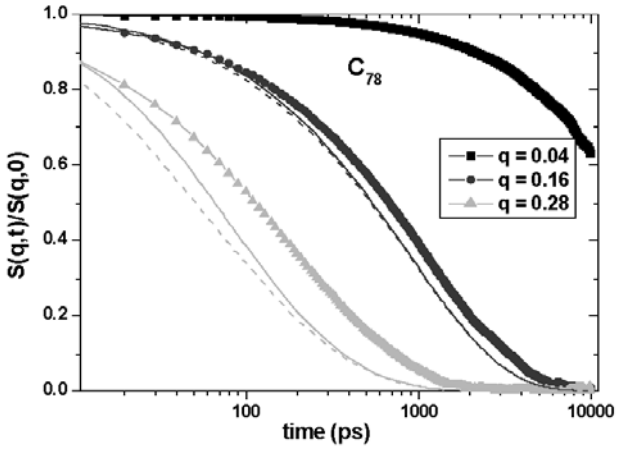

(b)

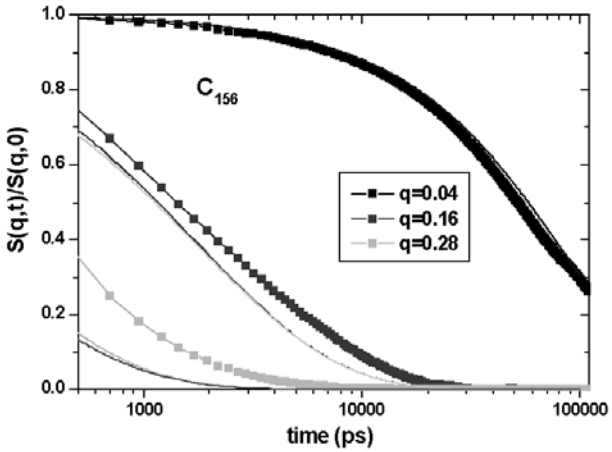

Figure 2. Normalized single-chain dynamic structure factor $S(q,t)/S(q,0)$ obtained from the MD simulations (symbols) with the C_{78} and C_{156} PE systems, for various q values (0.04 Å^{-1}, 0.16 Å^{-1}, and 0.28 Å^{-1}). Shown with the solid lines are the predictions of the Rouse model and with the dashed ones those of the semiflexible chain model of Harnau *et al*.[3]

polymer segments along the chain does not follow the Rouse behavior. The reason for this is that these segments are too short for their end-to-end vector to follow a Gaussian distribution.[14] In this case, by accounting for rigidity effects, the semiflexible chain model of Harnau *et al*.[3] somewhat improves the agreement with simulation data, particularly at shorter times. Unfortunately, for considerably longer times the predictions of the semiflexible and the Rouse chain models become indistinguishable, both exhibiting significant deviations from the simulation data.

For the C_{156} PE system, the situation is different since systematic deviations are observed over the entire regime of wavevector lengths q studied,

particularly the higher ones. Thus, for this system, there is no q value in the interval [0.04 Å^{-1} - 0.4 Å^{-1}] for which some kind of agreement with the Rouse model can be established. These deviations become larger for the C_{1000} PE melt (results not shown in Figures 2 and 3) suggesting that other processes and mechanisms (than those captured by the Rouse model) govern its dynamics. To elucidate this, in Figure 3, we have analyzed the dynamic structure factor for the C_{1000} PE melt on the basis of the reptation model restricting ourselves to the regime of q values for which eq. (16) is applicable, i.e., in the interval $1/\sqrt{\langle R^2 \rangle} << q/2\pi << 1/\alpha$. If we borrow an estimate for the effective tube diameter from reported experimental data for high molecular weight PE melts[2] ($a \cong$ 35-45 Å), and use that $<R^2> \cong$ 19,500 Å^2 for the C_{1000} PE melt, then the regime of q values for which eq. (16) can be used is $0.045<<q<<0.16$. [Note here that for the PE system, C_{156}, it was impossible to identify such a regime due to its significantly smaller $<R^2>$ value]. $S(q,t)$-vs.-t graphs for the C_{1000} melt corresponding to two such q values (equal to 0.08 Å^{-1} and 0.10 Å^{-1}, respectively) are shown in Figure 3. The symbols in the figure describe the data obtained directly from the MD simulations (symbols) while the lines indicate the predictions of the reptation theory based on the use of eq. (16). The latter have been obtained by fitting the equation to the simulation data using as the only free parameter the value of the effective tube diameter α. The values of the other two parameters that appear in the equation, the friction factor ζ governing the short time scale τ_0 and the disentanglement time τ_d, were

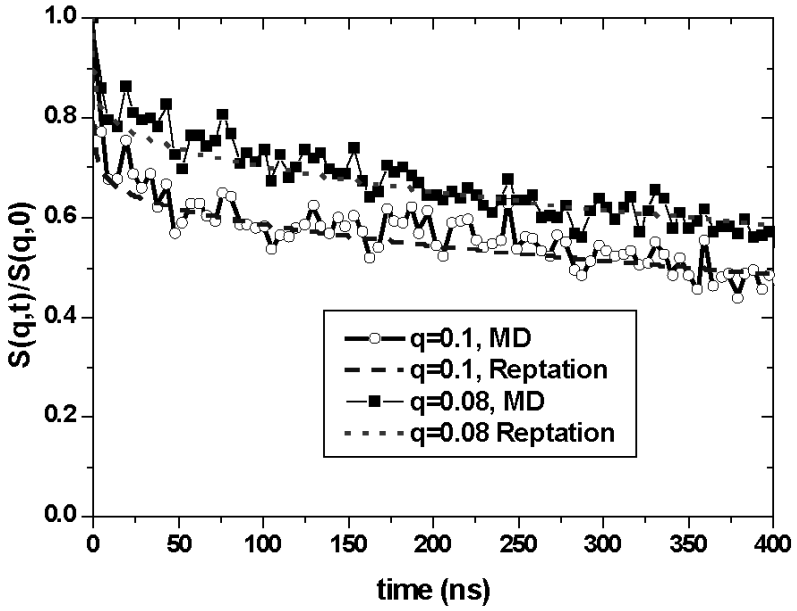

Figure 3. $S(q,t)/S(q,0)$-vs.-t plots for the C_{1000} system and comparison with the predictions of the reptation theory, eq. (16) in the main text, for two q values, 0.08Å^{-1} and 0.10Å^{-1}.

calculated according to the methodology described in Ref. 16 as $\zeta \cong 4\text{x}10^{-10}$ dyn sec/cm, and $\tau_d \cong 4.5$ μs, respectively. ζ was extracted by mapping MD data for the chain self diffusion coefficient in the Rouse regime (e.g., for the C_{78} PE system) onto the Rouse model using also that its value should be chain-length independent (since it refers to one monomer along a PE chain), while τ_d was estimated by extracting a value for the chain self-diffusion coefficient in the C_{1000} PE melt from the msd of the chain centers-of-mass in the Fickian regime based on the Einstein relation ($D \approx 0.00013$Å^2/ps), and then using that $\tau_d = < R^2 > / 3\pi^2 D$.

With the above-mentioned values for ζ and τ_d, the simulation curves in Figure 3 were fitted to eq. (16) leaving the value of the effective tube diameter a as the only free parameter. This led to the data shown by the continuous lines in Figure 3, with the best-fit value for a equal to (55 ± 5) Å. As mentioned above, the corresponding experimental value for high molecular weight PE melts[2,36] is between 35 and 45 Å. The comparison is really very favorable considering also that C_{1000} is a rather short PE melt (molecular length approximately equal to 10 N_e) whereas the predictions of the classical reptation theory should hold for extremely high molecular weight systems (chain length ~ 100 N_e) due to the neglect of phenomena related to contour-length fluctuations and constraint release mechanisms (see also Ref. 36).

C. Mean-square displacement of chain segments

Figure 4 reports logarithmic plots of the segmental mean-square displacements in the three PE systems calculated by monitoring the time evolution of the innermost segments along the chain that are free of chain end effects,[17] as

$$g(t) = \frac{1}{2n+1} \sum_{i=N/2-n}^{N/2+n} \left(\mathbf{R}(i,t) - \mathbf{R}(i,0) \right)^2 \qquad (18)$$

with n the number of innermost segments monitored (here, n=4, which means that only the dynamics of the nine most inner segments in any chain in the system were tracked). Three different curves are displayed in the Figure, corresponding to the three model PE systems, C_{78}, C_{156} and C_{1000}. The dashed one refers to the C_{78} PE melt which is seen to obey quite well the scaling laws of the Rouse model: it is characterized by a short time behavior where $\phi(n,t) \sim t^{1/2}$, followed by the long time (or Fickian diffusion) regime where $\phi(n,t) \sim t^1$. In fact, due to the non-negligible contribution of the linear term in eq. (8) in this time scale, the slope of the short-time part of the curve is slightly higher than 0.5, close to 0.6. It is also interesting that the end of this short-time behavior is located at $t \approx 2$ ns, which is practically the Rouse time for the C_{78} melt.[14] Also shown in the Figure are the curves corresponding to the C_{156} (dotted line) and the C_{1000} (solid line) PE melts.

Focusing, in particular, on the curve representing the data for the C_{1000} system, one clearly identifies the 3 distinct breaks (marked by the three arrows) characteristic of a system following reptation dynamics. The corresponding exponents in the scaling of $\phi(n,t)$ with t are equal to 0.55, 0.30, 0.55, and 0.90, respectively, indeed very close to those predicted by the reptation theory (equal to 0.50, 0.25, 0.50 and 1.00, respectively). The reasons for the small deviations (recorded mainly in the two intermediate regions of the plot should be sought to the approximations of negligible contour length fluctuations and tube constraint mechanisms involved in the original reptation theory, which is not the case for the relatively short chain length C_{1000} PE system analyzed here. Similar results have been found from MD simulations using coarse-grained models.[37,38]

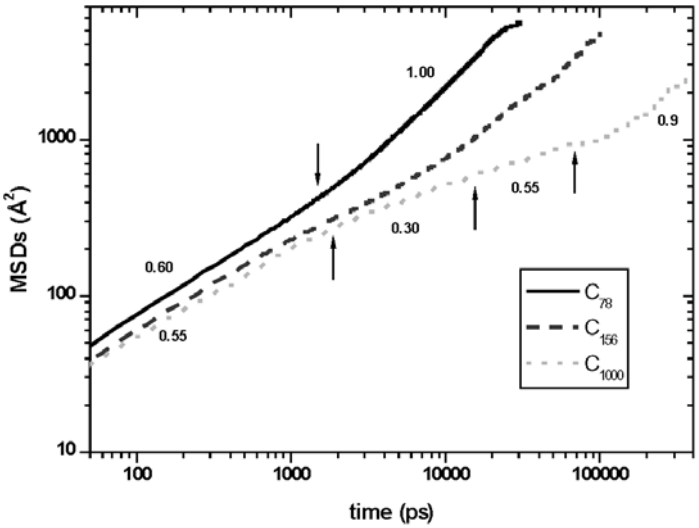

Figure 4. Mean-square displacement $g(t)$ of the innermost segments versus time t in a log-log plot in the three systems.

D. Normal modes

Figure 5 displays results about the characteristic relaxation spectrum in the C_{78} and C_{156} PE systems. For the third system (C_{1000}) which follows reptation dynamics, the normal mode analysis should be carried out in terms of the curvilinear primitive path coordinates and this will be the subject of a future analysis.[39] The results have been obtained by calculating the autocorrelation function (ACF) of each normal mode, $\langle \mathbf{X}_p(t)\cdot\mathbf{X}_p(0)\rangle$, in the course of the MD simulation and then by fitting them with stretched exponential (KWW) functions of the form:

$$\left\langle \mathbf{X}_p(t)\ .\ \mathbf{X}_p(0)\right\rangle = A_p \exp\left(-\frac{t}{t_p}\right)^{\beta_p} \tag{19}$$

where t_p and β_p are the characteristic relaxation time and stretching exponent parameters, respectively, for the given mode. A_p, on the other hand, is the amplitude accounting for the very fast decay in the very short time regime. The corresponding total correlation times τ_p (equal to the integrals below each curve) are then obtained by using that $\tau_p = \frac{t_p}{\beta_p}\Gamma\left(\frac{1}{\beta_p}\right)$.

Figure 5 presents results for the normalized relaxation spectrum $p^2\tau_p/\tau_1$ in the two systems, as a function of mode number p. According to the Rouse model, relaxation times should scale as $\tau_p \sim 1 / p^2$ (see eq. (6)), so all points in Figure 5 should have fallen on the same straight line (the line with value 1). The situation in Figure 5 is a little different: the normalized times $p^2\tau_p/\tau_1$ depend on the number of the normal mode, i.e., they indicate a departure from the scalings of the Rouse model. Given that the p-th normal mode corresponds to the dynamics of a polymer segment of length equal to N/p, such a departure (which has also been reported in the past[13,14,26]) should be related to the non-Gaussian conformation of the shorter segments (as also mentioned in section IV.B above). It is interesting, though, that for both systems (C_{78} and C_{156}), except for the first 3 normal modes, $p_2\tau_p/\tau_1$ for all higher modes retains a constant value equal to 0.8 ± 0.1. A similar trend was observed very recently also for *cis*-1,4-polybutadiene where the coordinates with mode number p higher than 3 were found to obey exactly the same scaling: $p^2\tau_p/\tau_1 \cong 0.70$.[26]

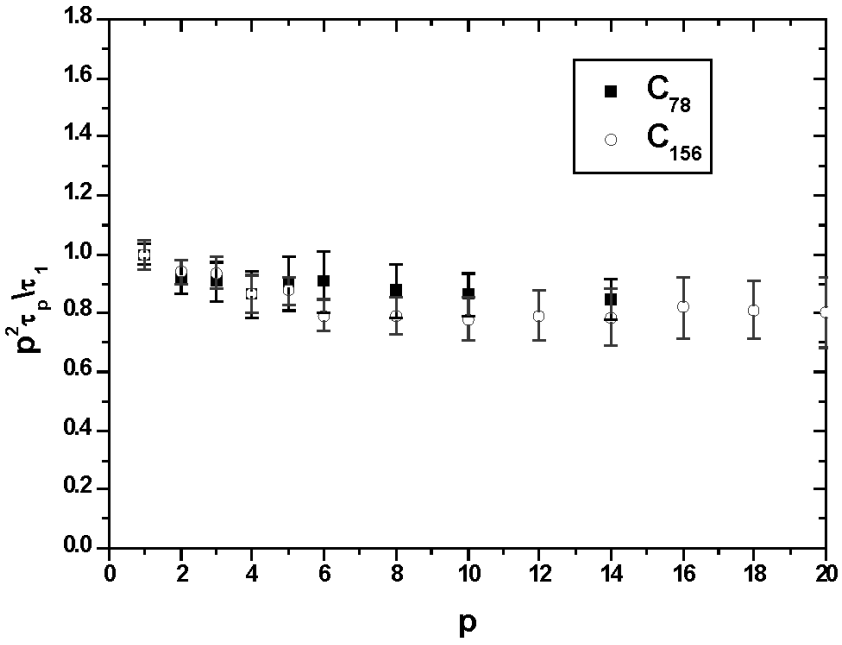

Figure 5. Results of normal mode analysis: scaling of the $p^2\tau_p/\tau_1$ ratio with mode number p for the C_{78} and C_{156} PE melts.

This is very important because it can be used to extract the maximum relaxation time, τ_1, for systems and/or conditions where τ_1 is not readily accessible by the atomistic MD simulation. In Ref. 26, for example, such a strategy was used to get estimates of the Rouse time in a *cis*-1,4-polybutadiene system at temperatures close to its glass transition temperature (where the backbones of the polymer chains are practically frozen but where motions associated with smaller units along the chain remain active) and compute its fragility index.

V. Conclusions - Outlook

We have presented results for the dynamic properties (with an emphasis on segmental mobility) of three linear PE melts characterized by mean chain lengths equal to C_{78}, C_{156} and C_{1000}, respectively, obtained from atomistic MD simulations carried out for times up to 0.5 μs. Four different measures of segmental dynamics and motion were analyzed, related to conformational and normal mode relaxation, segmental msd, and single chain dynamic structure factor. How segmental dynamics in the three systems is related to the predictions of the well-known mesoscopic Rouse and reptation models (each one in its own regime of validity) was also analyzed and discussed.

The most significant results of this work are: (a) the evaluation of the effective tube diameter for the C_{1000} system through an accurate fit of its $S(q,t)$ spectrum with an analytical expression derived on the assumptions of the reptation theory, using as input simulation data for the monomer friction coefficient ζ and the disentanglement time τ_d, and (b) the proposition for a modified scaling of the characteristic relaxation spectrum of the Rouse normal modes of the form $p^2\tau_p/\tau_1 \cong 0.70$ for all modes $\mathbf{X}_p$ with p greater than about 3.

In the future, our efforts will focus on a detailed analysis of the primitive path dynamics in the C_{1000} PE system with an emphasis on the correlation between reptation (defining the probability $\psi(s,t)$ that a segment s along the chain remains in the tube after time t) and the relaxation of the chain tangent vectors $\mathbf{u}(s,t)$ and the chain end-to-end vector $\mathbf{R}$.

References

1. Ferry, J. D. *Viscoelastic Properties of Polymers*; J. Wiley & sons: New York, 1980; Berry, G. C.; Fox, T. G. *Adv. Polym. Sci.* **1968**, *5*, 261.
2. Doi, M.; Edwards, S. F. *The Theory of Polymer Dynamics*; Clarendon Press: Oxford, 1986.
3. Harnau, L.; Winkler, R.G.; Reineker, P. *J. Chem. Phys.* **1955**, *102*, 7750; **1996**, *104*, 6355.
4. Schleger, P.; Farago, B.; Lartigue, C.; Kollmar, A.; Richter, D. *Phys. Rev. Lett.* **1998**, *81*, 124.

5 Richter, D.; Willner, L.; Zirkel, A.; Farago, B.; Fetters L.J.; Huang, J.S. *Macromolecules* **1994**, *27*, 7437.
6. Richter, D.; Farago, B.; Fetters L.J.; Huang, J.S.; Ewen, B.; Lartigue, C. *Phys. Rev. Lett*. **1990**, *64*, 1389.
7. Moe, N.E.; Qiu, X.H.; Ediger, M.D. *Macromolecules* **2000**, *33*, 2145.
8. Qiu, X.H.; Moe, N.E.; Ediger, M.D.; Fetters. L.J. *J. Chem. Phys*. **2000**, *113*, 2918.
9. Lippow, S.M.; Qiu, X.H.; Ediger, M.D. *J. Chem. Phys.* **2001**, *115*, 4961.
10. Paul, W.; Smith, G. D.; Yoon, D. Y.; Farago, B.; Rathgeber, S.; Zirkel, A.; Willner, L.; Richter, D. *Phys. Rev. Lett.* **1998**, *80*, 2346.
11. Graft, R.; Heuer, A.; Spiess, H.W. *Phys. Rev. Lett*. **1998**, *80*, 5738.
12. Paul, W.; Smith, G. D.; Yoon, Do Y. *Macromolecules* **1997**, *30*, 7772.
13. Mondello, M.; Grest, G. *J. Chem. Phys.* **1997**, *106*, 9327.
14. Harmandaris, V.A.; Mavrantzas, V.G.; Theodorou, D.N. *Macromolecules* **1998**, *31*, 7934.
15. Harmandaris, V.A.; Doxastakis, M. ; Mavrantzas, V.G.; Theodorou, D.N. *J. Chem. Phys.* **2002**, *116*, 436.
16. Harmandaris, V.A.; Mavrantzas, V.G.; Theodorou, D.N., Kröger, M.; Ramirez, J.; Öttinger, H.C.; Vlassopoulos, D. *Macromolecules* **2003**, *36*, 1376.
17. Harmandaris, V.A.; Mavrantzas, V.G. in *Simulation Methods for Polymers*, eds. Theodorou, D.N. and Kotelyanskii; Marcel Dekker, New York, 2004.
18. Tsolou, G.; Mavrantzas, V.G.; Theodorou, D.N. *Macromolecules* **2005**, *38*, 1478.
19. Ahumada, O.; Theodorou, D.N.; Triolo, A.; Arrighi, V.; Karatasos, C.; Ryckaert, J.-P. *Macromolecules* **2002**, 35, 7110.
20. Doxastakis, M.; Kitsiou, M.; Fytas, G.; Theodorou, D.N.; Hadjichristidis, N.; Meier, G.; Frick, B. *J. Chem. Phys*. **2000**, *112*, 8687.
21. Antoniadis, S.J.; Samara, C.T.; Theodorou, D.N. Macromoleculs 1999, 32, 8635.
22. Borodin, O.; Smith, G.D. *Macromoleculs* **2000**, *33*, 2273.
23. Smith, G.D.; Borodin, O.; Bedrov, D.; Paul, W.; Qiu, X.H.; Ediger, M.D. *Macromolecules* **2001**, *34*, 5192.
24. Smith, G. D.; Paul, W.; Monkenbush, M.; Richter, D. *Chem. Phys.* **2000**, *261*, 61.
25. Karayiannis, N.Ch.; Mavrantzas, V.G. *Macromolecules* **2005**, *38*, 8583.
26. Tsolou, G.; Harmandaris, V.A.; Mavrantzas, V.G. *J. Non-Newt. Fluid Mech.* **2007**, accepted.
27. Van der Ploeg P.; Berendsen, H. J. *J. Chem. Phys*. **1982**, *76*, 3271.
28. Ryckaert J.P.; Bellemans, A. *Chem. Phys. Lett.* **1975**, *30*, 123.
29. Ryckaert, J.P.; Ciccoti, G.; Berendsen, H.J.C. *J. Comp. Phys.* **1977**, *101*, 327.
30. Martyna, G.J.; Tuckerman, M.E.; Tobias, D.J.; Klein, M.L. *Mol. Phys.* **1996**, *87*, 1117.
31. Mavrantzas, V.G.; Boone, T.D.; Zervopoulou, E.; Theodorou, D.N. *Macromolecules* **1999**, *32*, 5072.
32. Everaers, R.; Sukumaran, S.K.; Grest, G.S.; Svaenborg, C.; Sivasubramanian, A.; Kremer, K. *Science* **2004**, *43*, 917.
33. Kröger, M. *Comput. Phys. Commun.* **2005**, *168*, 209.
34. Tzoumanekas, C.; Theodorou, D.N. *Macromolecules* **2006**, *39*, 4592.
35. De Gennes, P.G. *J. Physique* **1981**, *42*, 735.
36. Wischnewski, A.; Monkenbusch, M.; Willner, L.; Richter, D.; Likhtman, A.E.; McLeish, T.C.B.; Farago, B. *Phys. Rev. Lett.* **2002**, *88*, 058301.

37. Kremer, K.; Grest, G.S. *J. Chem. Phys*. **1990**, *92*, 5057.
38. Pütz, M.; Kremer, K.; Grest, G.S. *Europhys. Lett*. **2000,** *49*, 735.
39. Harmandaris, V.A.; Mavrantzas, V.G. unpublished results.